THE JOURNAL OF PHYSICAL CHEMISTRY B
A JOURNAL OF THE AMERICAN CHEMICAL SOCIETY

pubs.acs.org/JPCB

Article

Controlling the Ion Transport Number in Solvent-in-Salt Solutions

Ivan Popov,* Airat Khamzin, Ray A. Matsumoto, Wei Zhao, Xiaobo Lin, Peter T. Cummings, and Alexei P. Sokolov*

Cite This: *J. Phys. Chem. B* 2022, 126, 4572−4583

Read Online

ACCESS | Metrics & More | Article Recommendations

ABSTRACT: Solvent-in-salt (SIS) systems present promising materials for the next generation of energy storage applications. The ion dynamics is significantly different in these systems from that of ionic liquids and diluted salt solutions. In this study, we analyze the ion dynamics of two salts, Li-TFSI and Li-FSI, in highly concentrated aqueous and acetonitrile solutions. We performed high-frequency dielectric measurements covering the range of up to 50 GHz and molecular dynamics simulations. The analysis of the conductivity spectra provides the characteristic crossover time between individual charge rearrangements and the normal charge diffusion regime resulting in DC conductivity. Analysis revealed that the onset of normal charge diffusion occurs at the scale of ∼1.5−3.5 Å, comparable to the average distance between the ions. Based on the idea of momentum conservation, distinct ion correlations were estimated experimentally and computationally. The analysis revealed that cation−anion correlations can be suppressed by changing the solvent concentration in SIS systems, leading to an increase of the light ion (Li^+ in our case) transport number. This discovery suggests a way for improving the light cation transport number in SIS systems by tuning the solvent concentration.

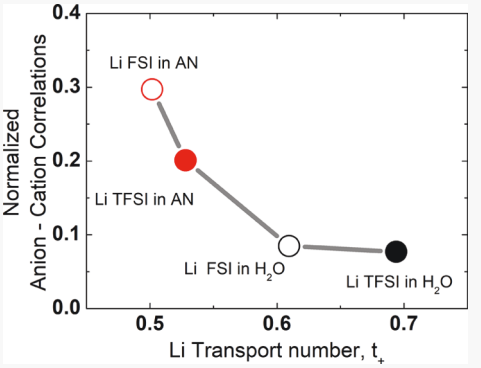

I. INTRODUCTION

Solvent-in-salt (SIS) systems, i.e., highly concentrated salt electrolytes, attracted significant attention in recent years.[1−6] They are considered as promising candidates for the next generation of batteries and supercapacitors due to their improved properties, such as high cation transport number,[7−9] high electrochemical stability,[10,11] suppression of lithium dendrite formation,[12] less flammability, less volatility, and high charge density.[3,10,13] However, the cost of all these impressive properties is a decrease in conductivity,[8,14,15] which might be an obstacle for widespread applications of SIS systems. Ion diffusion and ion−ion and ion−solvent correlations are the critical parameters controlling the ionic conductivity. Thus, the fundamental understanding of the mechanisms controlling charge transport in SIS systems is critical for their rational design and implementation in energy storage applications.

Many interesting properties in SIS systems were revealed in recent years,[3,8,9,14,16−21] where the presence of a small amount of solvent makes their dynamics and structure significantly different from those of ionic liquids and diluted salt solutions. Especially, the aqueous solutions or water-in-salt (WIS) systems were in the spotlight of several recent publications.[7−11,16,17,20,22] It was shown that in WIS systems, the electrochemical stability window of water significantly increases;[10] at the same time, these systems still demonstrate high DC conductivity.[8,14] Molecular dynamics (MD) simulations and experiments revealed a disproportion in cation and anion solvation in WIS electrolytes resulting in the formation of a liquid structure with nano-heterogeneity.[8,14] The nanoheterogeneity leads to the formation of water-rich channels acting like conducting wires for lithium ion transport.[9,14] Moreover, later papers show that in highly concentrated Li-TFSI aqueous systems, the anion also plays a significant role in the extended H-bonding network to facilitate Li transport,[23] leading to an increase of the lithium transport number. However, other studies demonstrate that in the same system, the water network is completely broken and is replaced by a $TFSI^-$ network.[24,25] Furthermore, recent studies revealed surprisingly strong acidity in highly concentrated Li-TFSI aqueous solutions,[26] which was ascribed to the deprotonation of the water molecules bridged to lithium ions. All these results indicate a completely different behavior of the solvent in highly concentrated electrolytes. It is worth noting that if water is replaced with acetonitrile (AN), the liquid structure becomes less heterogeneous,[8,14] and the effect of the high lithium transport number disappears at the same salt molar concentration.[14] Another interesting aspect is the study of the ion−ion correlations in SIS systems. Obviously, the reduction of the solvent in electrolytes results in a decrease of the distance

Received: March 31, 2022
Revised: May 27, 2022
Published: June 10, 2022

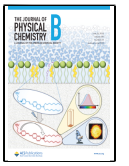

https://doi.org/10.1021/acs.jpcb.2c02218
J. Phys. Chem. B 2022, 126, 4572−4583

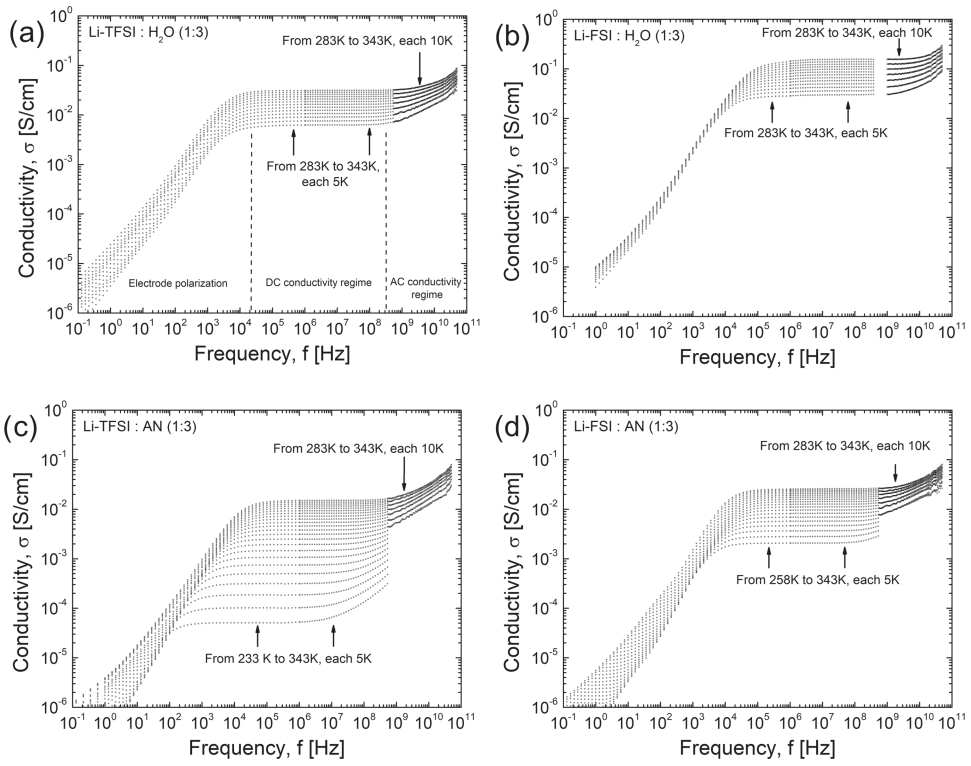

Figure 1. Wide frequency spectra of conductivity for different salt solutions with molar concentration $\nu_{salt}/\nu_{solvent}$ = 1:3: (a) Li-TFSI in water, (b) Li-FSI in water, (c) Li-TFSI in acetonitrile, and (d) Li-FSI in acetonitrile. In (a), the usual regimes are shown: (i) AC conductivity, (ii) DC conductivity, and (iii) electrode polarization effect.

between the ions and higher interactions and correlations between them.

Thus, the SIS systems have very distinct properties in comparison to those of the diluted electrolytes and "solvent-free" ionic liquids. However, the microscopic dynamic properties of ions in SIS systems remain poorly studied experimentally. The quasielastic neutron scattering (QENS) technique, which can provide detailed information on the geometry and time scale of individual ion jumps,[27] so far was not efficient due to hydrogen atoms of solvent molecules dominating the QENS signal. The QENS study of the highly concentrated aqueous Li-TFSI electrolyte revealed much slower water dynamics in comparison to that of bulk water,[22] but no information on ion dynamics was extracted due to the small neutron cross sections of Li-TFSI in comparison to water molecules. In this respect, broadband dielectric spectroscopy (BDS)[28] can give valuable information because it measures the response from the diffusion of charge carriers.

In this study, we measured conductivity spectra from below 1 Hz to ∼50 GHz in highly concentrated Li-TFSI and Li-FSI solutions in water and acetonitrile. Analysis of the data using the random barrier model[29−33] suggests significant heterogeneity in the studied SIS systems. Moreover, the presented analysis revealed that the ions reach the diffusion regime already at a distance of ∼1.5−3.5 Å, comparable to the distance between ions. Using this model, we were able to estimate the ion diffusion at low temperatures not accessible to the NMR technique and to estimate the correlations in ion dynamics, i.e., the inverse Haven ratio. Furthermore, we analyzed the distinct ionic contributions to conductivity, based on the momentum conservation law and MD simulations. The most interesting is that our analysis revealed that a change in the solvent concentration can suppress the anion−cation contribution to conductivity and increase the Li^+ transport number, and the dependence of the transport number on the solvent concentration is defined by the ion−solvent dynamic correlations. The discovered behavior suggests an interesting avenue in the design of liquid electrolytes with a high cation transport number.

II. EXPERIMENTAL RESULTS

II.I. Materials. Li-TFSI and Li-FSI salts were purchased from Sigma-Aldrich and TCI America and were mixed in molar fractions $\nu_{salt}/\nu_{solvent}$ = 1:3 with distilled water and anhydrous acetonitrile (AN). Both salts are stable in AN; however, Li-FSI is reasonably stable in water only at temperatures below 50 °C.[14] Detailed analysis of the Li-FSI stability is presented in ref 34. To avoid any artifacts related to the salt decomposition, all the studied solutions were prepared right before the experimental measurements.

II.II. Conductivity Spectral Measurements. Conductivity spectral measurements were performed using three spectrometers to cover the wide frequency range from 0.1 Hz up to 50 GHz. An α-A analyzer from Novocontrol was utilized in the frequency range of 10^{-1}−10^6 Hz. A cell consists of a cap as a bottom electrode; the upper electrode is separated from the cap using a sapphire window to avoid electrical contact between them. The fixed electrode distance of 0.4 mm and diameter of 10.2 mm were used. The samples were measured with a voltage amplitude of 0.1 V. The standard calibration procedure was used before measurements. An Agilent RF impedance material analyzer, E4991A, with WinDETA Software from Novocontrol was used in the frequency range of 10^6−3×10^9 Hz. The cell was constructed from two APC-7 connectors. For the upper electrode, the inner pin of one connector was replaced with a

https://doi.org/10.1021/acs.jpcb.2c02218
J. Phys. Chem. B 2022, 126, 4572−4583

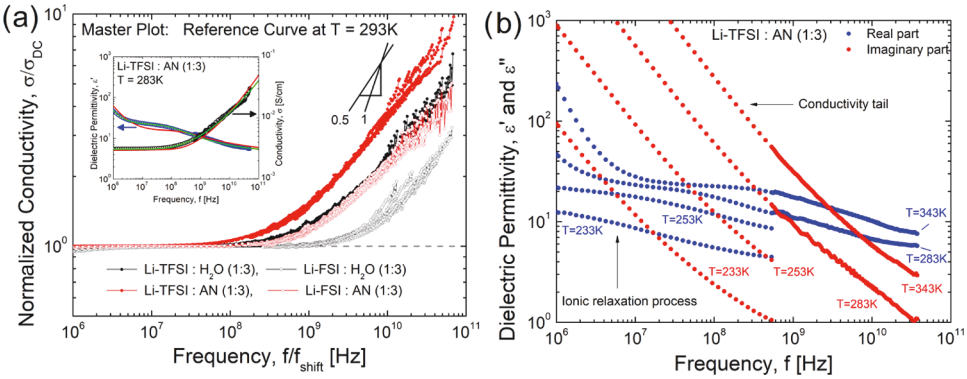

Figure 2. (a) Master plot of conductivity, where spectra were normalized by DC conductivity and to the position of the reference curve (at $T = 293$ K). The inset is a demonstration of data fitting by eq 1 (red line) and eq 2 (green line). (b) Spectra of real and imaginary parts of dielectric permittivity for the Li-TFSI in AN ($\nu_{salt}/\nu_{solvent}$ = 1:3).

solid pin with a diameter of 3 mm, and the free space between the inner pin and outer part was filled with Teflon. For the lower electrode, the pin in another connector was removed, and in the free central space, a movable metallic cylinder was inserted. As a result, the coaxial line was terminated with the plate capacitor with an adjustable distance between the electrodes. The coaxial line was calibrated using a standard procedure (Open/Short/50 Ohm) to move the reference plane up to the cell, terminating the line. The cell was calibrated as well (Open and Short) for better precision. The samples were loaded between the two electrodes with a distance of 0.1 mm and measured with a voltage amplitude of 0.1 V. A panoramic network analyzer, Agilent Technologies, E8364C, with a 85070E dielectric probe kit was utilized for frequency measurements from 5×10^8 Hz up to 5×10^{10} Hz. A performance probe with the Agilent electronic calibration module (ECal) was used for measurements of the real and imaginary parts of dielectric permittivity. The calibration was performed in a standard procedure using Open, Short (performance probe kit), and Load (distilled water at 20 °C) states. Just before each measurement, the calibration was refreshed using the ECal module. A Quattro temperature controller (Novocontrol) was used for temperature stabilization for the measurements from 10^{-1} to 10^9 Hz. The samples were stabilized for 20 min at each temperature to reach a precision of ±0.2 K. A Julabo Presto W80 was used together with a homemade cryofurnace for temperature stabilization for the measurements from 5×10^8 Hz up to 5×10^{10} Hz. The samples were stabilized for 40 min at each temperature to reach a precision of ±0.2 K.

The conductivity spectra for all studied systems exhibit three usual regions (Figure 1a–d): (i) frequency-dependent alternating current (AC) conductivity regime at high frequencies, σ_{AC}; (ii) a plateau level of the direct current (DC) conductivity regime at the intermediate frequency range, σ_{DC}, and (iii) a decrease due to the accumulation of charge carriers at the surface of the electrode at lower frequency (electrode polarization effect).[35]

II.III. Molecular Dynamics Simulations. Classical molecular dynamics (MD) simulations were performed using GROMACS 2020.[36] The all-atom optimized potential for the liquid system (OPLS-AA) force field[37] was used to describe Li^+ ions and acetonitrile (AN), and the SPC/E model was used to describe water. The force field parameters of $TFSI^-$ ions were taken from ref 38. All the bonds with the hydrogen atoms were constrained by the LINCS algorithm.[39] In Li-TFSI solutions, the molar ratio of Li-TFSI to solvent is 1:3, which is consistent with experiments. The PACKMOL software package[40] was used to put a certain number of molecules at random nonoverlapping positions. The steepest-descent energy minimization was first performed to relax any initial unfavorable interactions. Then, MD simulations were performed using the isothermal–isobaric (NPT) ensemble. The systems were further equilibrated in the canonical (NVT) ensemble for 10 ns. To calculate the ion–ion, ion–solvent, and solvent–solvent correlations, the production simulations were performed for 1 ns. A timestep of 1fs was used, and the configurations were saved every 10 fs. The temperature was maintained at 303 K through a Nosé–Hoover thermostat,[41,42] and a Berendsen barostat[43] was used to control the pressure at 1 bar. A cutoff length of 1.2 nm was employed for the van der Waals interactions and Columbic interactions in the real space. The long-range electrostatic interactions were calculated by the particle mesh Ewald (PME) method with a minimum grid spacing of 0.1 nm in the inverse space.[44] Five independent simulations with different initial configurations were used to achieve sufficient sampling for each system. To generate more accurate dynamic properties of salt ions in solvents, we compared the mean square displacement (MSD, $|r_i(t) - r_i(0)|^2$, where $r_i(t)$ refers to the center of mass positions of ions) from MD with experimental data, and the partial charges for salt ions were scaled by a factor of 0.85 (see Figure 3c) from MD simulations with experiments. Production run for 8 ns in the NPT ensemble was used to generate MSD. The system pressure was controlled using a Parrinello–Rahman barostat[45,46] at 1 bar. The diffusivity of salt ions in the solvent was calculated by the Einstein relation: $D = \lim_{t\to\infty} \frac{1}{6t}\langle[r_i(t) - r_i(0)]^2\rangle$. The total ion–ion autocorrelation conductivity was derived from the autocorrelation function of electric current through the Green–Kubo relation[47] $\sigma = \frac{1}{3k_BTV}\int_0^\infty \langle\vec{J}(t)\cdot\vec{J}(0)\rangle dt$, where k_B, T, and V refer to the Boltzmann constant, temperature, and system volume, respectively. $\vec{J}(t)$ is the electric current $\vec{J}(t) = e\sum_{(i=1)}^{N} z_i\vec{v}(t) = e\sum_{(i_+=1)}^{(N_+)} z_+\vec{v}_{i+}(t) + e\sum_{i-=1}^{N} z_-\vec{v}_{i-}(t)$, where e, N, z, and $\vec{v}$ refer to the elementary charge, number of ions, and velocity of ions and "−/+" denotes the anion/cation, respectively. The total ion–ion autocorrelation conductivity is represented in the sum of six different partial autocorrelation conductivities by employing the autocorrelation function between different or the same species,[48] $\sigma = \sigma_{s,+} + \sigma_{d,+} + \sigma_{s,-} + \sigma_{d,-} + \sigma_{+,-} + \sigma_{-,+}$, where "s/d" denotes self- and distinct correlations, respectively. The solvent–

https://doi.org/10.1021/acs.jpcb.2c02218
J. Phys. Chem. B 2022, 126, 4572–4583

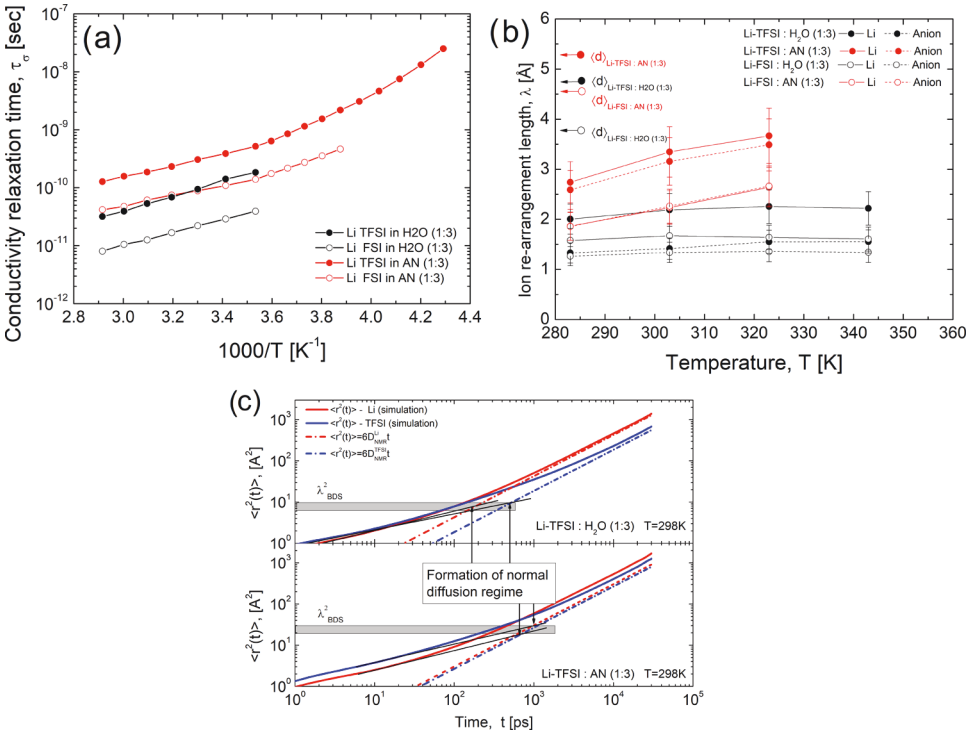

Figure 3. (a) Conductivity relaxation time obtained from eq 2. (b) Ion rearrangement length obtained from eq 3. The average distance between the ions, ⟨d⟩, for the corresponding systems is shown by arrows. (c) MD simulation of mean square displacement for cations and anions (Li-TFSI in H_2O and AN systems). The dashed lines represent $\langle r^2(t)\rangle = 6D_{NMR}t$. The gray rectangles show the value range of square of the rearrangement length, λ^2, found from conductivity spectra and plotted in (b). The cross of black lines corresponding to the slope of $\langle r^2(t)\rangle$ in the anomalous diffusion regime with the line of the normal diffusion regime indicating the length and time scale, where transition from the anomalous to the normal diffusion regime occurs.

solvent autocorrelation diffusivity and ion−solvent autocorrelation diffusivity were calculated by the time integral of the velocity autocorrelation function $D = \int_0^\infty \langle \vec{v}_i(t)\cdot\vec{v}_{solvent}(0)\rangle dt$, where i stands for the solvent, cation, or anion molecules.

III. DATA ANALYSIS

III.I. Analysis of the Conductivity Spectra. As in many ionic systems,[31,32] the time−temperature superposition for AC−DC crossover holds well also for SIS systems (Figure 2a), and all the conductivity data collapse well into a master curve by scaling conductivity by σ_{DC} and frequency by f_{shift}. The master curve presents a crossover from the power law behavior of AC conductivity at high frequencies to the plateau level of DC conductivity at lower frequencies. A broad conductivity relaxation process appears in the real part of the dielectric permittivity around the same AC−DC crossover frequency (Figure 2b). This process is always covered by the DC conductivity tail in the imaginary part of the dielectric permittivity (Figure 2b).

The random barrier model (RBM)[29−32] is often used to describe the conductivity spectra. This model suggests that the transport of charge carriers happens by hops over potential energy barriers. In this case, with a constant barrier height distribution, the model leads to the equation[29]

$$\frac{\sigma^*(\omega)}{\sigma_{DC}}\ln\left(\frac{\sigma^*(\omega)}{\sigma_{DC}}\right) = i\omega\tau_\sigma \quad (1)$$

Here, $\sigma^*(\omega)$ is the complex conductivity; σ_{DC} is the DC conductivity; and τ_σ is the conductivity relaxation time. The latter defines the characteristic AC−DC crossover time, i.e., when the charge subdiffusive regime, $\langle r^2(t)\rangle \sim t^\alpha$ with $\alpha < 1$, crosses over to a normal diffusion regime, $\langle r^2(t)\rangle \sim t$ (here, $\langle r^2(t)\rangle$ is the charge mean-squared displacement). Eq 1 describes not only the conductivity spectra but also the conductivity relaxation process in the real part of the dielectric permittivity. The validity of eq 1 was tested in computer simulations, and it was shown that if the system is highly inhomogeneous, eq 1 provides an inaccurate fit of the simulation data at high frequencies. Based on the idea of the fractal percolating cluster, the correction term was introduced to fix this drawback, and eq 1 was revised[33]

$$\ln\left(\frac{\sigma^*(\omega)}{\sigma_{DC}}\right) = \frac{i\omega\tau_\sigma\sigma_{DC}}{\sigma^*(\omega)}\left(1 + \frac{8}{3}\frac{i\omega\tau_\sigma\sigma_{DC}}{\sigma^*(\omega)}\right)^{-1/3} \quad (2)$$

It was shown that eq 2 describes well the conductivity spectra of polyionic and molecular ionic liquids.[49,50] Moreover, it was suggested that using the diffusion coefficient, D, independently measured from PFG-NMR, the characteristic length of the crossover to Fickian diffusion can be estimated[49−52]

$$\lambda = \sqrt{6D\tau_\sigma} \quad (3)$$

Analysis of ionic liquids revealed $\lambda \sim 2$−3 Å, and it was ascribed to the ion jump length.[52,53] However, analysis of polyionic liquids (PolyILs) revealed $\lambda \sim 4$−7 Å,[49] which is too large for a single ion jump in a condensed matter. This length was ascribed to the characteristic distance the ion needs to move to escape from a Coulombic cage formed by the neighboring ions.[49,50] Depending on the size of the Coulombic cage, the ion

https://doi.org/10.1021/acs.jpcb.2c02218
J. Phys. Chem. B 2022, 126, 4572−4583

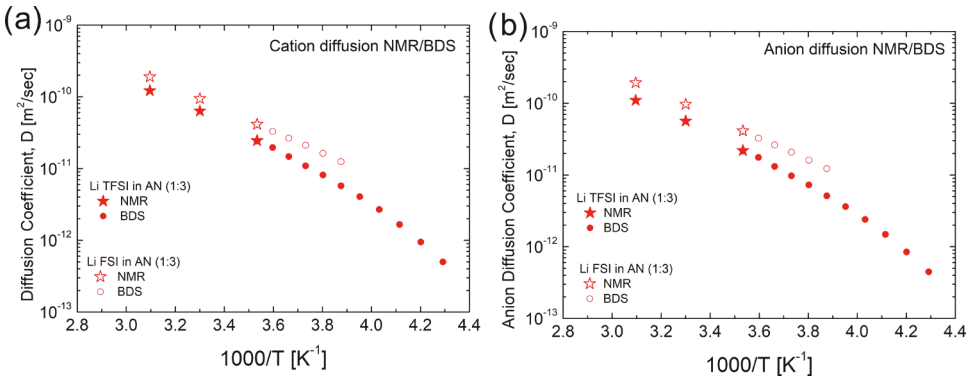

Figure 4. Diffusion coefficient for the cations (a) and anions (b) measured by PFG-NMR[14] (stars) and BDS (dots) for Li-TFSI/FSI in the AN system.

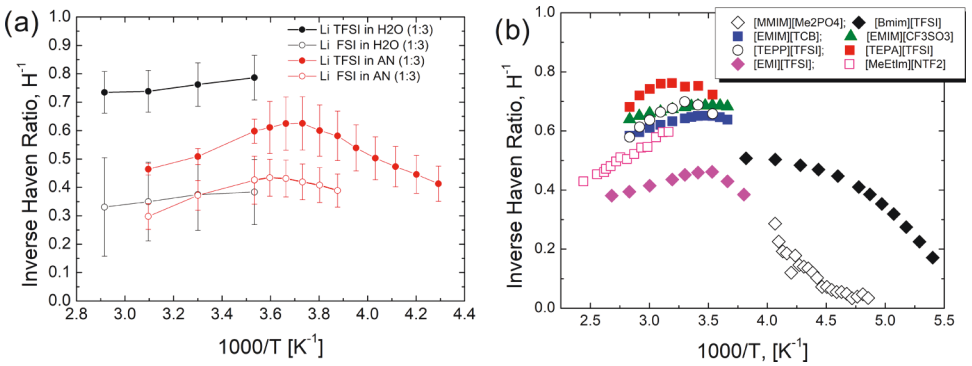

Figure 5. (a) Ionicity or inverse Haven ratio. The data at high temperature were taken from ref 14 and those for Li-TFSI in AN ($\nu_{salt}/\nu_{solvent}$ = 1:3) at low temperature were calculated based on the diffusion coefficient from Figure 3a. (b) Temperature dependence of H^{-1} for various ILs (data from refs 49, 52, 74−77, some recalculated from the estimates of "free ion" concentration). The data clearly show the existence of the maximum at some specific temperatures.

might have several elementary jumps, a kind of rattling in the Coulombic cage, before escaping from it.[49,50] This escape leads to ion rearrangements and a reorientation of dipole moments and appears as conductivity (ionic) relaxation in $\varepsilon^*(\omega)$ with relaxation time, τ_σ. It was also suggested that knowing parameter λ and using τ_σ from the BDS measurements, one can estimate the ion diffusion coefficient in the lower temperature range not accessible to NMR.[49]

However, the idea mentioned above was tested only for polyionic and molecular ionic liquids.[49−52] Applying the same approach to the SIS systems studied here revealed that eq 2 provides better fit of the data than eq 1 (see the inset of Figure 2a). This result indicates high inhomogeneity of the SIS systems, which was suggested earlier based on the MD simulations[8] and FTIR studies.[9,14] The temperature dependence values of the conductivity are published in our previous work;[14] the temperature dependence values of the ionic relaxation time, τ_σ, are presented in Figure 3a. Using diffusion of ions measured with PFG-NMR[14] and eq 3, we estimated the ion rearrangement length: $\lambda_+ = \sqrt{6D_+\tau_\sigma}$ and $\lambda_- = \sqrt{6D_-\tau_\sigma}$. The obtained values of the ion rearrangement length are in the range of 1−3 Å (Figure 3b). In agreement with an earlier suggestion,[49] this distance is indeed approximately half the average distance between the ions $\langle d\rangle = [(3/4\pi n)^{1/3}]/2$ (Figure 3b), where n is the ion pair concentration. We also note that the estimated ion rearrangement length is comparable to the jump length of solvent molecules measured independently by QENS in our previous work.[14] The MD simulations of mean square displacement also indicate (Figure 3c) that the crossover from the subdiffusive regime to the normal diffusion indeed appears at $\langle r^2(t)\rangle \sim \lambda^2$ and time equal to τ_σ (as a cross of extrapolated lines corresponding to the slope of $\langle r^2(t)\rangle$ in the anomalous diffusion regime with the line of the normal diffusion regime).

Knowing the $\lambda_\pm$ parameter, it is possible to estimate the diffusion coefficient at low temperatures, not accessible to PFG-NMR measurements. For this purpose, we can rewrite eq 3 as follows: $D_\pm = \lambda_\pm^2/(6\tau_\sigma)$. For the AN system, the ion rearrangement length depends slightly on the temperature, and we used the minimum value of $\lambda_\pm$ at low temperature to estimate the diffusion coefficient. The results including also the PFG-NMR measurements from our previous work[14] are presented in Figure 4. The results for aqueous solution are not shown because of its crystallization at low temperature.

III.II. Ionic Correlations in SIS Systems. Knowing the ion diffusion from NMR and conductivity relaxation time, we can estimate the expected ionic conductivity using the Nernst−Einstein (NE) equation[49,54−56]

$$\sigma_{NE} = \frac{q^2 n}{k_B T}(D_+ + D_-) \tag{4}$$

where q is an ion charge and D_+^{self} and D_-^{self} are the anion and cation diffusion coefficients, respectively. The NE equation assumes independent (uncorrelated) contribution of ions to conductivity. However, in concentrated ionic systems, ion−ion interactions lead to strong correlations in the dynamics of the ions and failure of the NE equation.[49,52,55,57−68] The ratio of the measured DC conductivity and estimated uncorrelated

https://doi.org/10.1021/acs.jpcb.2c02218
J. Phys. Chem. B 2022, 126, 4572−4583

conductivity via eq 4 is called the ionicity or inverse Haven ratio[58,62,67−73]

$$H^{-1} = \frac{\sigma_{DC}}{\sigma_{NE}} \tag{5}$$

The inverse Haven ratio for all four studied systems is less than one (Figure 5a), which corresponds to the negative effect of ion−ion correlations suppressing the conductivity. Furthermore, it appears that the inverse Haven ratio has a nonmonotonous variation with a maximum at some temperatures. A similar maximum in the inverse Haven ratio was previously reported for some solvent-free ionic liquids (Figure 5b).[49,52,74−77] To the best of our knowledge, the origin of the maximum in the temperature dependence of the inverse Haven ratio was not discussed in the literature. Earlier studies[51,78,79] ascribed the variation of the inverse Haven ratio (or ionicity) at low temperatures to the dissociation energy of ion pairs. Although we know now that $H^{-1} < 1$ in ILs is not due to ion pairs,[57] electrostatic interactions between ions, E_{el}, still control the strength of ionic interactions and H^{-1}. In that case, we would expect $H^{-1} \sim \exp(-E_{el}/k_BT)$, explaining the decrease in H^{-1} at lower temperatures. The decrease of H^{-1} at higher temperatures in some ILs was ascribed to a change in hydrophobic interactions and ion aggregations.[80] It is also possible that the nanoheterogeneity existing in SIS systems[8,9] might depend on the temperature, affecting ion−ion correlations. In particular, analysis of our results for the characteristic length of ion rearrangements (Figure 3b) reveals a weak temperature variation of λ in acetonitrile-based SIS systems and almost no variations in aqueous SIS systems. This correlates to a much stronger high temperature decrease of H^{-1} in acetonitrile-based SIS systems (Figure 5a). Although these ideas might provide some qualitative explanation for the temperature dependence of the ionic correlations reflected in the inverse Haven ratio, the detailed mechanism of these temperature variations remains unclear and requires additional study.

IV. ION−ION CORRELATIONS IN SIS SYSTEMS

To understand the mechanism of the ionic correlations and their contributions to the conductivity, we need to go to the basic definitions of diffusion and conductivity. The diffusion coefficient of ions is defined by the velocity−velocity self-correlation function[54−56]

$$D = \frac{1}{3}\int_0^\infty \langle \bar{v}(0)\cdot\bar{v}(t)\rangle \mathrm{d}t \tag{6}$$

while the conductivity is generally defined by the current−current correlation function that depends on velocity−velocity correlations of all the ions[54−56]

$$\sigma_{DC} = \frac{1}{3Vk_BT}\int_0^\infty \langle \bar{J}(0)\cdot\bar{J}(t)\rangle \mathrm{d}t, \text{ where } \langle \bar{J}(0)\cdot\bar{J}(t)\rangle = \left\langle \sum_i q_i\bar{v}_i(0)\cdot\sum_j q_j\bar{v}_j(t)\right\rangle \tag{7}$$

Only in the case with no correlations between different ions, i.e., $\langle \vec{v}_i(0)\vec{v}_j(t)\rangle = \delta_{ij}\langle \vec{v}(0)\cdot\vec{v}(t)\rangle$ (δ_{ij} is the Kronecker delta), eq 7 reduces to NE eq 4. In general, we can separate the ionic conductivity (eq 7) into four terms[48,57,81]

$$\sigma_{DC} = \sigma_{NE} + \sigma_{++} + \sigma_{--} + \sigma_{+-},\ \sigma_{NE} = \sigma_+^s + \sigma_-^s \tag{8}$$

Here, σ_+^s and σ_+^s represent the contribution from the self-correlation of cations and anions, respectively; σ_{++} and σ_{--} are the distinct cation−cation and anion−anion correlations, respectively; and σ_{+-} is the contribution of cation−anion correlations to the conductivity. Hence, the inverse Haven ratio can be defined as

$$H^{-1} = 1 + \frac{\sigma_{+-}}{\sigma_{NE}} + \frac{\sigma_{++}}{\sigma_{NE}} + \frac{\sigma_{--}}{\sigma_{NE}} \tag{9}$$

Direct experimental measure of the contribution of each term in eq 9 to the H^{-1} is a challenging problem.[82] However, we can apply the approach proposed by Schönert,[81] which is based on the idea of momentum conservation between all the mobile components of the systems. This model has been applied to ionic liquids,[48,83] PolyILs, and plastic crystals,[57] showing reasonable results. However, the SIS systems have a third component, solvent molecules, and the final equations derived in refs 48, 57 should be modified to account for their contribution to the momentum conservation. The Appendix section presents a detailed derivation of the distinct ion−ion correlations based on the momentum conservation law (A.4), following the procedure presented in ref 48. As it is shown in the Appendix, the result depends on the relationship between distinct cation−solvent (D_{+s}^d) and anion−solvent (D_{-s}^d) correlations. For the case of $D_{+s}^d = -D_{-s}^d$, we have

$$\sigma_{+-} = \frac{2m_-m_+}{(m_- + m_+)^2}\left[\sigma_{DC} + \frac{e^2n}{k_BT}\frac{\nu_{solvent}}{\nu_{salt}}\frac{m_s^2}{m_+m_-}(D_s^{self} + D_{ss}^d)\right],\ \text{if } D_{+s}^d = -D_{-s}^d$$

$$\sigma_{++} = \frac{m_-^2}{(m_- + m_+)^2}\left[\sigma_{DC} - \frac{e^2n}{k_BT}\frac{(m_- + m_+)^2}{m_-^2}D_+^{self} - \frac{e^2n}{k_BT}\frac{\nu_{solvent}}{\nu_{salt}}\frac{m_s^2}{m_-^2}\frac{(m_+ + 3m_-)}{(m_- - m_+)}(D_s^{self} + D_{ss}^d)\right]$$

$$\sigma_{--} = \frac{m_+^2}{(m_- + m_+)^2}\left[\sigma_{DC} - \frac{e^2n}{k_BT}\frac{(m_- + m_+)^2}{m_+^2}D_-^{self} + \frac{e^2n}{k_BT}\frac{\nu_{solvent}}{\nu_{salt}}\frac{m_s^2}{m_+^2}\frac{(m_- + 3m_+)}{(m_- - m_+)}(D_s^{self} + D_{ss}^d)\right] \tag{10}$$

However, in the case *of* $D_{+s}^d = -D_{-s}^d$, we obtain the next relationship for distinct ion−ion correlations

$$\sigma_{+-} = \frac{2m_-m_+}{(m_- + m_+)^2}\left[\sigma_{DC} - \frac{e^2n}{k_BT}\frac{\nu_{solvent}}{\nu_{salt}}\frac{m_s^2}{m_+m_-}(D_s^{self} + D_{ss}^d)\right],\ \text{if } D_{+s}^d = D_{-s}^d$$

$$\sigma_{++} = \frac{m_-^2}{(m_- + m_+)^2}\left[\sigma_{DC} - \frac{e^2n}{k_BT}\frac{(m_- + m_+)^2}{m_-^2}D_+^{self} + \frac{e^2n}{k_BT}\frac{\nu_{solvent}}{\nu_{salt}}\frac{m_s^2}{m_-^2}(D_s^{self} + D_{ss}^d)\right]$$

$$\sigma_{--} = \frac{m_+^2}{(m_- + m_+)^2}\left[\sigma_{DC} - \frac{e^2n}{k_BT}\frac{(m_- + m_+)^2}{m_+^2}D_-^{self} + \frac{e^2n}{k_BT}\frac{\nu_{solvent}}{\nu_{salt}}\frac{m_s^2}{m_+^2}(D_s^{self} + D_{ss}^d)\right] \tag{11}$$

Here, $m_\pm$ and $D_\pm^{self}$ are the masses and self-diffusion coefficients of cations/anions, respectively, m_s and D_s^{self} are the mass and self-diffusion coefficient of the solvent, D_{ss}^d is the distinct diffusion coefficient of the solvent, and $\nu_{solvent}/\nu_{salt}$ is the molar solvent/salt ratio.

Analysis of correlations in our MD simulations predicts that for the systems studied here, $D_{+s}^d > 0$, indicating the formation of the hydration shell around Li^+ that moves together with this

https://doi.org/10.1021/acs.jpcb.2c02218
J. Phys. Chem. B 2022, 126, 4572−4583

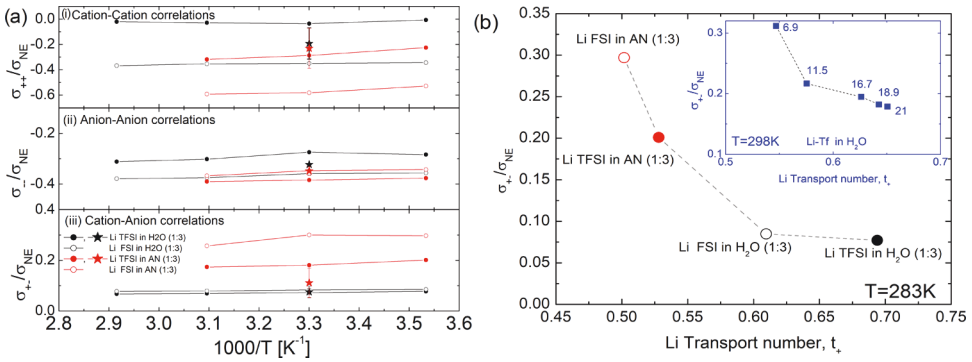

Figure 6. (a) Temperature dependence of contributions of (i) cation−cation, (ii) anion−anion, and (iii) anion−cation correlations to the inverse Haven ratio based on eq 10 (circles). MD simulations are shown by star symbols. (b) Contribution of anion−cation correlations to the inverse Haven ratio versus Li transport number. The diffusion coefficients for the anion, cation, and solvent were taken from ref 14. The inset is the same dependence but for the Li-Tf in water; the data were taken from ref 19.

cation. The simulations also indicate that $D^{d}_{+s} \approx -D^{d}_{-s}$, corresponding to eq 10. In this case, the parameter $\sigma_{\pm}$ is always positive ($\sigma_{\pm} > 0$), regardless of the amount of the solvent. This result is in line with the paper,[20] where the MD simulations were done also for Li-TFSI in water and it was predicted that anion−solvent and cation−solvent correlations have an opposite sign and that the distinct anion−cation diffusion coefficient is always negative (which is equivalent to positive anion−cation conductivity, $\sigma_{+-} > 0$) in the whole solvent concentration range. Our MD simulations also show that the value of the solvent self-diffusion coefficient is more than 5 times larger than the distinct solvent diffusion coefficient, and the latter can be neglected ($D^{self}_{s} \gg D^{d}_{ss}$). Using eq 10, we can analyze the temperature dependence of all distinct ionic correlations (Figure 6a). It can be seen that all distinct ion−ion correlations do not show any significant temperature variations; however, they show a good agreement with the simulated result, confirming the validity of the proposed model, eq 10.

The most interesting result is a potential relationship between the cation transport number, $t_+ = D^{self}_{+}/(D^{self}_{+} + D^{self}_{-})$, and normalized anion−cation correlations, σ_{+-}/σ_{NE} (which define the contribution of distinct anion−cation correlations to the inverse Haven ratio). Our analysis reveals a surprising result (Figure 6b): the decrease in σ_{+-}/σ_{NE} in SIS systems studied here correlates to an increase in the Li^+ transport number. The t_+ is larger for the Li-TFSI in H_2O, where σ_{+-}/σ_{NE} is the smallest. On the contrary, normalized anion−cation correlations are the strongest for Li-FSI in AN, and the diffusion of cations and anions equalized, leading to $t_{Li} \to 0.5$. To verify the generality of this result, we did the same analysis for the aqueous solutions of Li-Tf studied in ref 19 and found a similar behavior at different salt concentrations (inset of Figure 6b). Using the first equation in (10), we can present it in the next form

$$\frac{\sigma_{+-}}{\sigma_{NE}} = \frac{2m_-m_+}{(m_- + m_+)^2}\left[H^{-1} + \frac{\nu_{solvent}}{\nu_{salt}}\frac{m_s^2}{m_+m_-}\frac{D^{self}_{s}}{D^{self}_{+} + D^{self}_{-}}\right], \quad \text{if } \begin{matrix} D^{d}_{+s} = -D^{d}_{-s} \\ D^{self}_{s} \gg D^{d}_{ss} \end{matrix} \tag{12}$$

This equation suggests that if the inverse Haven ratio does not change much with solvent concentrations and diffusion of the solvent, cations and anions have similar solvent dependence values (i.e., ratio of $D^{self}_{s}/[D^{self}_{+} + D^{self}_{-}]$ is constant or depends weakly on the solvent concentration), and the contribution of the anion−cation increases with addition of the solvent. According to the findings presented in Figure 6b, this should lead to a decrease of the cation transport number. This also explains the results presented in ref 8, where it was shown that the transport number of Li decreases with the solvent increase in systems with different salts and solvents, while the inverse Haven ratio and $D^{self}_{s}/(D^{self}_{+} + D^{self}_{-})$ depend weakly on the solvent concentration (at least for Li-TFSI in water).

According to eq 10, it is impossible to reach $\sigma_{+-} = 0$ because both terms for σ_{+-} are positive. However, in the case of $D^{d}_{+s} = D^{d}_{-s}$ according to eq 11, anion−cation correlations change the sign depending on the solvent concentration: In the absence of the solvent, the contribution from $\sigma_{\pm}$ is always positive, while it might become negative at a high solvent content, if the second term prevails over the first one. It is in agreement with the previously published simulations in refs 48, 82, 84. Kashyap et al.[48] demonstrated that in solvent-free molten salt, $D_{\pm} \propto -\sigma_{\pm}$ is negative, while in diluted salt solution, $D_{\pm} > 0$. In the paper of McDaniel et al.[84] the MD simulations were conducted for the $[BMIM^+][BF_4]$ IL in different solutions, and it was shown that in neat ionic liquid, $\sigma_{\pm} > 0$, while at high solvent concentrations, $\sigma_{\pm} < 0$ in all solutions. A similar result was obtained by Dong et al.[82] for the Li-TFSI in tetraglyme, where term $\sigma_{\pm}$ also changes the sign from slightly negative in dilute solutions to highly positive in concentrated salt electrolytes.

As mentioned above, in the systems where eq 11 is valid, the cation−anion correlations might reach zero at a specific solvent concentration and become negative in dilute solutions. According to the findings presented in Figure 6b, this should lead to an increase in the transport number of the lightest ion in dilute solutions. Indeed, according to the simulation results presented in ref 84, σ_{+-} is positive in the neat BMIM-BF_4 ionic liquids but becomes negative in dilute solutions. As a result, the transport number of the lighter ion BF_4 constantly increases with the increase in the solvent content in ref 84, in agreement with the correlations discovered here. In this case, apparently relatively large ions in this IL do not form a hydration shell with any of the solvent studied, providing no preferential solvent−ion correlations with one of the ions.

Thus, the current model based on the momentum conservation law might explain the controversy between recent results[48,82,84] and ref 20 demonstrating different signs of anion−cation correlations and different behaviors of the transport number versus solvent content. These studies, actually, simulated different systems, where ion−solvent interactions

https://doi.org/10.1021/acs.jpcb.2c02218
J. Phys. Chem. B 2022, 126, 4572−4583

are different and cation−solvent and anion−solvent correlations might have the same or opposite signs, which leads to different behaviors in $\sigma_{\pm}$.

Summarizing based on this observation and analysis of the literature data, we can formulate an important hypothesis: *For the electrolytes where anion−solvent and cation−solvent correlations have opposite signs (i.e., obeying eq 10), the transport number of the lightest ion decreases with the solvent content increase, while for the systems where anion−solvent and cation−solvent correlations have the same sign (i.e., obeying eq 11), the transport number of the lightest ion increases with the solvent content increase.* This is an empirical observation, which follows the momentum conservation law. However, it is worth noting that in eqs 10 and 11, there is an interplay between the first and second terms, and not always increasing the solvent content leads to an increase of cation−anion correlations for systems (10) and decrease in systems (11). So far, the proposed hypothesis is validated only on a few systems and might explain several literature results. Therefore, to make the hypothesis more general, it requires additional molecular dynamics and experimental verification. On the microscopic side, this difference in behavior might be explained by the formation of a hydration shell around one of the ions (the case described by eq 10), which slows down this ion diffusion but also decorrelates its motion with the motion of the counter ion. However, in the case when both ions have no hydration shell, i.e., their distinct correlations with the solvent are similar (the case described by eq 11), anion−cation correlations might change the sign with the increase of the solvent concentration.

V. CONCLUSIONS

In the current research, the conductivity relaxation model was tested and validated in SIS systems. This approach provides estimates of the ion rearrangement length and time scale where ion mean-squared displacement crosses over from the subdiffusion regime to normal diffusion. This length in the studied SIS systems is comparable to the average distance between the ions and to the solvent jump length estimated from QENS. This result suggests that ion rearrangements in these concentrated systems might happen in a single ion jump. Our analysis emphasizes strong heterogeneity in SIS systems. The model also provides a way to estimate the ion diffusion at low temperatures, which is not accessible to PFG-NMR techniques. It enables the analysis of the inverse Haven ratio in a broad temperature range. This analysis reveals a nonmonotonous temperature dependence of the inverse Haven ratio, the nature of which remains a puzzle.

The most interesting results are obtained from the analysis of distinct ion correlations, based on the momentum conservation law. This analysis explicitly accounts for the role of solvent−ion correlations in SIS systems and reveals that a decrease in anion−cation correlations leads to a higher transport number of the lightest ion. It appears that the amplitude of the cation−anion correlations can be tuned by changing the solvent concentration. This effect, however, depends on whether cation−solvent and anion−solvent distinct diffusion coefficients have the same or opposite signs. These results suggest an interesting way to increase the transport number of light cations in SIS systems.

■ APPENDIX A

Based on the idea of the momentum conservation approach of Schönert,[81] we present the contribution of distinct ion−ion correlations to the measured DC conductivity in the case of a three-component system (cation, anion, solvent). To derive these relationships in a simple form, we follow the procedure presented in ref 48. The conductivity is defined by eq 7; separating the contribution of cations and anions, we can rewrite eq 7 as follows

$$\sigma_{DC} = \frac{e^2}{3k_BTV}[z_+^2\sum_{i_+=1}^{N_+}\sum_{j_+=1}^{N_+}\int_0^\infty <\overline{v}_{i_+}(t)\cdot\overline{v}_{j_+}(0) > dt + z_-^2\sum_{i_-=1}^{N_-}\sum_{j_-=1}^{N_-}\int_0^\infty <\overline{v}_{i_-}(t)\cdot\overline{v}_{j_-}(0) > dt + 2z_+z_-\sum_{i_+=1}^{N_+}\sum_{j_-=1}^{N_-}\int_0^\infty <\overline{v}_{i_+}(t)\cdot\overline{v}_{j_-}(0) > dt] \quad (A.1)$$

where $z_{\pm}$ and $N_{\pm}$ are the charge numbers and number of mobile corresponding ions, respectively. Then, we consider the local area around the ion with the number of cations $\varphi_+ \gg 1$ and number of anions $\varphi_- \gg 1$ and make an assumption that inside this area, the ion correlations do not depend on the distance, while outside this area, the ion correlations are equal to zero. Assuming that all ions are mobile, $N_+ = N_- = N_{/2}$, and $\varphi_+ = \varphi_- = \varphi_{/2}$; from A.1, we have

$$\sigma_{DC} = \sigma_{NE} + \sigma_{++} + \sigma_{--} + \sigma_{+-},\ \sigma_{NE} = \frac{e^2n}{k_BT}(z_+^2D_+^{self} + z_-^2D_-^{self})$$
$$\sigma_{++} = \frac{e^2n}{k_BT}\frac{z_+^2D_{++}^d}{2},\ \sigma_{--} = \frac{e^2n}{k_BT}\frac{z_-^2D_{--}^d}{2},\ \sigma_{+-} = \frac{e^2n}{k_BT}z_+z_-D_{+-}^d \quad (A.2)$$

where n is the ion pair concentration and $D^{self/d}$ represents self and distinct diffusion coefficients.

$$D_+^{self} = \frac{1}{3}\int_0^\infty <\overline{v_+}(t)\cdot\overline{v_+}(0) > dt,$$
$$D_-^{self} = \frac{1}{3}\int_0^\infty <\overline{v_-}(t)\cdot\overline{v_-}(0) > dt$$
$$D_{++}^d = \frac{\varphi}{3}\int_0^\infty <\overline{v_+}(t)\cdot\overline{v_+'}(0) > dt,$$
$$D_{--}^d = \frac{\varphi}{3}\int_0^\infty <\overline{v_-}(t)\cdot\overline{v_-'}(0) > dt$$
$$D_{+-}^d = \frac{\varphi}{3}\int_0^\infty <\overline{v_+}(t)\cdot\overline{v_-}(0) > dt = \frac{\varphi}{3}\int_0^\infty <\overline{v_-}(t)\cdot\overline{v_+}(0) > dt \quad (A.3)$$

where the quotation at the plus/minus sign means the distinct anion/cation. At initial time, we can write the momentum conservation law in the case of the three-component system

$$m_+\sum_{j_+=1}^{N_+}\overline{v}_{j_+}(0) + m_-\sum_{j_-=1}^{N_-}\overline{v}_{j_-}(0) + m_s\sum_{j_s=1}^{N_s}\overline{v}_{j_s}(0) = 0 \quad (A.4)$$

where s-index denotes the solvent. Multiplying eq A.4 by $\overline{V}_{i+}(t)$, $\overline{V}_{i-}(t)$, and $\overline{V}_{is}(t)$ at a time, averaging, and integrating over the time, we obtain a system of three equations

$$m_+\left(D_+^{self} + \frac{D_{++}^d}{2}\right) + m_-\frac{D_{+-}^d}{2} + m_s\frac{\varphi_s}{\varphi}D_{+s}^d = 0$$
$$m_-\left(D_-^{self} + \frac{D_{--}^d}{2}\right) + m_+\frac{D_{+-}^d}{2} + m_s\frac{\varphi_s}{\varphi}D_{-s} = 0$$
$$m_s(D_s^{self} + D_{ss}^d) + m_+\frac{D_{+s}^d}{2} + m_-\frac{D_{-s}^d}{2} = 0 \quad (A.5)$$

where we introduce the self-diffusion coefficient of the solvent, D_s^{self}, distinct solvent−solvent, D_{ss}^d, solvent−anion, D_{+s}^d, and solvent−cation, D_{-s}^d, diffusion coefficients

https://doi.org/10.1021/acs.jpcb.2c02218
J. Phys. Chem. B 2022, 126, 4572−4583

$$D_s^{self} = \frac{1}{3}\int_0^\infty <\overline{v}_s(t)\overline{v}_s(0) > dt,\ D_{ss}^{d} = \frac{\varphi_s}{3}\int_0^\infty <\overline{v}_s(t)\overline{v}_{s'}(0) > dt$$
$$D_{+s}^{d} = \frac{\varphi}{3}\int_0^\infty <\overline{v}_+(t)\overline{v}_s(0) > dt,\ D_{-s}^{d} = \frac{\varphi}{3}\int_0^\infty <\overline{v}_-(t)\overline{v}_s(0) > dt \quad (A.6)$$

where φ_s is the number of the closest solvent molecules in the local area, where correlations are not equal to zero. At this stage, because the number of unknown variables is larger than the number of equations in eq A.5, we have to make an assumption to resolve the system eq A.5. Below, we consider two cases for ion−solvent correlations, which can be verified by MD simulations.

Case $D_{+s}^{d} \approx -D_{-s}^{d}$: In this case, the system of eq A.5 can be solved, and the next relationships for the distinct ion correlations can be obtained. In the case of $z_- = -1$ and $z_+ = 1$

$$D_{+-}^{d} = -\frac{4m_-m_+}{(m_- + m_+)^2}\left[\sigma_{DC}\frac{k_BT}{2e^2n} + \frac{\varphi_s}{\varphi}\frac{m_s^2}{m_-m_+}(D_s^{self} + D_{ss}^{d})\right]$$
$$D_{++}^{d} = \frac{4m_-^2}{(m_- + m_+)^2}\left[\sigma_{DC}\frac{k_BT}{2e^2n} - \frac{(m_- + m_+)^2}{2m_-^2}D_+^{self} - \frac{\varphi_s}{\varphi}\frac{m_s^2}{m_-^2}\frac{(m_+ + 3m_-)}{(m_- - m_+)}(D_s^{self} + D_{ss}^{d})\right]$$
$$D_{--}^{d} = \frac{4m_+^2}{(m_- + m_+)^2}\left[\sigma_{DC}\frac{k_BT}{2e^2n} - \frac{(m_- + m_+)^2}{2m_+^2}D_-^{self} + \frac{\varphi_s}{\varphi}\frac{m_s^2}{m_+^2}\frac{(m_- + 3m_+)}{(m_- - m_+)}(D_s^{self} + D_{ss}^{d})\right]$$
$$D_{+s}^{d} = -D_{-s}^{d} = \frac{2m_s(D_s^{self} + D_{ss}^{d})}{(m_- - m_+)} \quad (A.7)$$

Finally, introducing the molar concentration $\nu_{solvent}/\nu_{salt} = 2\varphi_s/\varphi$ and using eq A.2, we have

$$\sigma_{+-} = \frac{2m_-m_+}{(m_- + m_+)^2}\left[\sigma_{DC} + \frac{e^2n}{k_BT}\frac{\nu_{solvent}}{\nu_{salt}}\frac{m_s^2}{m_+m_-}(D_s^{self} + D_{ss}^{d})\right],$$
$$\sigma_{++} = \frac{m_-^2}{(m_- + m_+)^2}\left[\sigma_{DC} - \frac{e^2n}{k_BT}\frac{(m_- + m_+)^2}{m_-^2}D_+^{self} - \frac{e^2n}{k_BT}\frac{\nu_{solvent}}{\nu_{salt}}\frac{m_s^2}{m_-^2}\frac{(m_+ + 3m_-)}{(m_- - m_+)}(D_s^{self} + D_{ss}^{d})\right],$$
$$\sigma_{--} = \frac{m_+^2}{(m_- + m_+)^2}\left[\sigma_{DC} - \frac{e^2n}{k_BT}\frac{(m_- + m_+)^2}{m_+^2}D_-^{self} + \frac{e^2n}{k_BT}\frac{\nu_{solvent}}{\nu_{salt}}\frac{m_s^2}{m_+^2}\frac{(m_- + 3m_+)}{(m_- - m_+)}(D_s^{self} + D_{ss}^{d})\right] \quad (A.8)$$

Case $D_{+s}^{d} \approx D_{-s}^{d}$: In this case for $z_- = -1$ and $z_+ = 1$, we obtain next

$$D_{+-}^{d} = -\frac{4m_-m_+}{(m_- + m_+)^2}\left[\sigma_{DC}\frac{k_BT}{2e^2n} - \frac{\varphi_s}{\varphi}\frac{m_s^2}{m_-m_+}(D_s^{self} + D_{ss}^{d})\right]$$
$$D_{++}^{d} = \frac{4m_-^2}{(m_- + m_+)^2}\left[\sigma_{DC}\frac{k_BT}{2e^2n} - \frac{(m_- + m_+)^2}{2m_-^2}D_+^{self} + \frac{\varphi_s}{\varphi}\frac{m_s^2}{m_-^2}(D_s^{self} + D_{ss}^{d})\right]$$
$$D_{--}^{d} = \frac{4m_+^2}{(m_- + m_+)^2}\left[\sigma_{DC}\frac{k_BT}{2e^2n} - \frac{(m_- + m_+)^2}{2m_+^2}D_-^{self} + \frac{\varphi_s}{\varphi}\frac{m_s^2}{m_+^2}(D_s^{self} + D_{ss}^{d})\right]$$
$$D_{-s}^{d} = D_{+s}^{d} = -\frac{2m_s(D_s^{self} + D_{ss}^{d})}{m_- + m_+} \quad (A.9)$$

Finally, introducing the molar concentration $\nu_{solvent}/\nu_{salt} = 2\varphi_s/\varphi$ and using eq A.2, we have

$$\sigma_{+-} = \frac{2m_-m_+}{(m_- + m_+)^2}\left[\sigma_{DC} - \frac{e^2n}{k_BT}\frac{\nu_{solvent}}{\nu_{salt}}\frac{m_s^2}{m_+m_-}(D_s^{self} + D_{ss}^{d})\right],$$
$$\sigma_{++} = \frac{m_-^2}{(m_- + m_+)^2}\left[\sigma_{DC} - \frac{e^2n}{k_BT}\frac{(m_- + m_+)^2}{m_-^2}D_+^{self} + \frac{e^2n}{k_BT}\frac{\nu_{solvent}}{\nu_{salt}}\frac{m_s^2}{m_-^2}(D_s^{self} + D_{ss}^{d})\right],$$
$$\sigma_{--} = \frac{m_+^2}{(m_- + m_+)^2}\left[\sigma_{DC} - \frac{e^2n}{k_BT}\frac{(m_- + m_+)^2}{m_+^2}D_-^{self} + \frac{e^2n}{k_BT}\frac{\nu_{solvent}}{\nu_{salt}}\frac{m_s^2}{m_+^2}(D_s^{self} + D_{ss}^{d})\right] \quad (A.10)$$

AUTHOR INFORMATION

Corresponding Authors

Ivan Popov − *Chemical Sciences Division, Oak Ridge National Laboratory, Oak Ridge, Tennessee 37831, United States; Department of Chemistry, University of Tennessee, Knoxville, Tennessee 37996, United States;* orcid.org/0000-0002-7235-2043; Email: ipopov@utk.edu

Alexei P. Sokolov − *Chemical Sciences Division, Oak Ridge National Laboratory, Oak Ridge, Tennessee 37831, United States; Department of Chemistry, University of Tennessee, Knoxville, Tennessee 37996, United States;* orcid.org/0000-0002-8187-9445; Email: sokolov@utk.edu

Authors

Airat Khamzin − *Institute of Physics, Kazan Federal University, Kazan, Tatarstan 420008, Russia;* orcid.org/0000-0001-9741-4346

Ray A. Matsumoto − *Department of Chemical and Biomolecular Engineering, Vanderbilt University, Nashville, Tennessee 37235, United States;* orcid.org/0000-0002-9124-3512

Wei Zhao − *Department of Chemical and Biomolecular Engineering, Vanderbilt University, Nashville, Tennessee 37235, United States;* orcid.org/0000-0003-1497-9312

Xiaobo Lin − *Department of Chemical and Biomolecular Engineering, Vanderbilt University, Nashville, Tennessee 37235, United States*

Peter T. Cummings − *Department of Chemical and Biomolecular Engineering, Vanderbilt University, Nashville, Tennessee 37235, United States*

Complete contact information is available at: https://pubs.acs.org/10.1021/acs.jpcb.2c02218

Notes

The authors declare no competing financial interest.

■ ACKNOWLEDGMENTS

We thank Jeppe Dyre for helpful discussions. This work was supported by the Fluid Interface Reactions, Structures and Transport (FIRST) Center, an Energy Frontier Research Center funded by the U.S. Department of Energy, Office of Science, Office of Basic Energy Sciences. I.P. acknowledges partial financial support by the NSF (award CHE-2102425) for the data analysis. A.Kh. is thankful to the support by the Kazan Federal University Strategic Academic Leadership Program.

■ REFERENCES

(1) Li, M.; Wang, C.; Chen, Z.; Xu, K.; Lu, J. New Concepts in Electrolytes. *Chem. Rev.* **2020**, *120*, 6783−6819.
(2) Chen, S.; Zheng, J.; Mei, D.; Han, K. S.; Engelhard, M. H.; Zhao, W.; Xu, W.; Liu, J.; Zhang, J.-G. High-Voltage Lithium-Metal Batteries Enabled by Localized High-Concentration Electrolytes. *Adv. Mater.* **2018**, *30*, No. 1706102.
(3) Azov, V. A.; Egorova, K. S.; Seitkalieva, M. M.; Kashin, A. S.; Ananikov, V. P. "Solvent-in-salt" systems for design of new materials in chemistry, biology and energy research. *Chem. Soc. Rev.* **2018**, *47*, 1250−1284.
(4) Yamada, Y.; Wang, J.; Ko, S.; Watanabe, E.; Yamada, A. Advances and issues in developing salt-concentrated battery electrolytes. *Nat. Energy* **2019**, *4*, 269−280.
(5) Wang, J.; Yamada, Y.; Sodeyama, K.; Chiang, C. H.; Tateyama, Y.; Yamada, A. Superconcentrated electrolytes for a high-voltage lithium-ion battery. *Nat. Commun.* **2016**, *7*, No. 12032.
(6) Suo, L.; Hu, Y.-S.; Li, H.; Armand, M.; Chen, L. A new class of solvent-in-salt electrolyte for high-energy rechargeable metallic lithium batteries. *Nat. Commun.* **2013**, *4*, No. 1481.
(7) Yu, Z.; Curtiss, L. A.; Winans, R. E.; Zhang, Y.; Li, T.; Cheng, L. Asymmetric Composition of Ionic Aggregates and the Origin of High Correlated Transference Number in Water-in-Salt Electrolytes. *J. Phys. Chem. Lett.* **2020**, *11*, 1276−1281.
(8) Borodin, O.; Suo, L.; Gobet, M.; Ren, X.; Wang, F.; Faraone, A.; Peng, J.; Olguin, M.; Schroeder, M.; Ding, M. S.; et al. Liquid Structure with Nano-Heterogeneity Promotes Cationic Transport in Concentrated Electrolytes. *ACS Nano* **2017**, *11*, 10462−10471.
(9) Lim, J.; Park, K.; Lee, H.; Kim, J.; Kwak, K.; Cho, M. Nanometric Water Channels in Water-in-Salt Lithium Ion Battery Electrolyte. *J. Am. Chem. Soc.* **2018**, *140*, 15661−15667.
(10) Suo, L.; Borodin, O.; Gao, T.; Olguin, M.; Ho, J.; Fan, X.; Luo, C.; Wang, C.; Xu, K. "Water-in-salt" electrolyte enables high-voltage aqueous lithium-ion chemistries. *Science* **2015**, *350*, 938−943.
(11) Suo, L.; Oh, D.; Lin, Y.; Zhuo, Z.; Borodin, O.; Gao, T.; Wang, F.; Kushima, A.; Wang, Z.; Kim, H.-C.; et al. How Solid-Electrolyte Interphase Forms in Aqueous Electrolytes. *J. Am. Chem. Soc.* **2017**, *139*, 18670−18680.
(12) Jeong, S.-K.; Seo, H.-Y.; Kim, D.-H.; Han, H.-K.; Kim, J.-G.; Lee, Y. B.; Iriyama, Y.; Abe, T.; Ogumi, Z. Suppression of dendritic lithium formation by using concentrated electrolyte solutions. *Electrochem. Commun.* **2008**, *10*, 635−638.
(13) Dou, Q.; Lei, S.; Wang, D.-W.; Zhang, Q.; Xiao, D.; Guo, H.; Wang, A.; Yang, H.; Li, Y.; Shi, S.; Yan, X. Safe and high-rate supercapacitors based on an "acetonitrile/water in salt" hybrid electrolyte. *Energy Environ. Sci.* **2018**, *11*, 3212−3219.
(14) Popov, I.; Sacci, R. L.; Sanders, N. C.; Matsumoto, R. A.; Thompson, M. W.; Osti, N. C.; Kobayashi, T.; Tyagi, M.; Mamontov, E.; Pruski, M.; et al. Critical Role of Anion−Solvent Interactions for Dynamics of Solvent-in-Salt Solutions. *J. Phys. Chem. C* **2020**, *124*, 8457−8466.
(15) Seo, D. M.; Borodin, O.; Balogh, D.; O'Connell, M.; Ly, Q.; Han, S.-D.; Passerini, S.; Henderson, W. A. Electrolyte Solvation and Ionic Association III. Acetonitrile-Lithium Salt Mixtures−Transport Properties. *J. Electrochem. Soc.* **2013**, *160*, A1061−A1070.
(16) Han, S. Dynamic features of water molecules in superconcentrated aqueous electrolytes. *Sci. Rep.* **2018**, *8*, No. 9347.
(17) Han, S. Anionic effects on the structure and dynamics of water in superconcentrated aqueous electrolytes. *RSC Adv.* **2019**, *9*, 609−619.
(18) Han, S. Structure and dynamics in the lithium solvation shell of nonaqueous electrolytes. *Sci. Rep.* **2019**, *9*, No. 5555.
(19) Horwitz, G.; Rodríguez, C. R.; Steinberg, P. Y.; Burton, G.; Corti, H. R. Mobility-viscosity decoupling and cation transport in water-in-salt lithium electrolytes. *Electrochim. Acta* **2020**, *359*, No. 136915.
(20) Li, Z.; Bouchal, R.; Mendez-Morales, T.; Rollet, A. L.; Rizzi, C.; Le Vot, S.; Favier, F.; Rotenberg, B.; Borodin, O.; Fontaine, O.; Salanne, M. Transport Properties of Li-TFSI Water-in-Salt Electrolytes. *J. Phys. Chem. B* **2019**, *123*, 10514−10521.
(21) Yamada, Y.; Furukawa, K.; Sodeyama, K.; Kikuchi, K.; Yaegashi, M.; Tateyama, Y.; Yamada, A. Unusual Stability of Acetonitrile-Based Superconcentrated Electrolytes for Fast-Charging Lithium-Ion Batteries. *J. Am. Chem. Soc.* **2014**, *136*, 5039−5046.
(22) González, M. A.; Borodin, O.; Kofu, M.; Shibata, K.; Yamada, T.; Yamamuro, O.; Xu, K.; Price, D. L.; Saboungi, M.-L. Nanoscale Relaxation in "Water-in-Salt" and "Water-in-Bisalt" Electrolytes. *J. Phys. Chem. Lett.* **2020**, *11*, 7279−7284.
(23) Jeon, J.; Lee, H.; Choi, J.-H.; Cho, M. Modeling and Simulation of Concentrated Aqueous Solutions of LiTFSI for Battery Applications. *J. Phys. Chem. C* **2020**, *124*, 11790−11799.
(24) Zhang, Y.; Lewis, N. H. C.; Mars, J.; Wan, G.; Weadock, N. J.; Takacs, C. J.; Lukatskaya, M. R.; Steinrück, H.-G.; Toney, M. F.; Tokmakoff, A.; Maginn, E. J. Water-in-Salt LiTFSI Aqueous Electrolytes. 1. Liquid Structure from Combined Molecular Dynamics Simulation and Experimental Studies. *J. Phys. Chem. B* **2021**, *125*, 4501−4513.
(25) Zhang, Y.; Maginn, E. J. Water-In-Salt LiTFSI Aqueous Electrolytes (2): Transport Properties and Li+ Dynamics Based on Molecular Dynamics Simulations. *J. Phys. Chem. B* **2021**, *125*, 13246−13254.
(26) Han, K. S.; Yu, Z.; Wang, H.; Redfern, P. C.; Ma, L.; Cheng, L.; Chen, Y.; Hu, J. Z.; Curtiss, L. A.; Xu, K.; et al. Origin of Unusual Acidity and Li+ Diffusivity in a Series of Water-in-Salt Electrolytes. *J. Phys. Chem. B* **2020**, *124*, 5284−5291.
(27) Singwi, K. S.; Sjölander, A. Diffusive Motions in Water and Cold Neutron Scattering. *Phys. Rev.* **1960**, *119*, 863−871.
(28) Kremer, F.; Schönhals, A. *Broadband Dielectric Spectroscopy*; Springer Science & Business Media, 2002.
(29) Dyre, J. C. The random free-energy barrier model for ac conduction in disordered solids. *J. Appl. Phys.* **1988**, *64*, 2456−2468.
(30) Dyre, J. C. Studies of ac hopping conduction at low temperatures. *Phys. Rev. B* **1994**, *49*, 11709−11720.
(31) Dyre, J. C.; Schrøder, T. B. Universality of ac conduction in disordered solids. *Rev. Mod. Phys.* **2000**, *72*, 873−892.
(32) Schrøder, T. B.; Dyre, J. C. Scaling and Universality of ac Conduction in Disordered Solids. *Phys. Rev. Lett.* **2000**, *84*, 310−313.
(33) Schrøder, T. B.; Dyre, J. C. ac Hopping Conduction at Extreme Disorder Takes Place on the Percolating Cluster. *Phys. Rev. Lett.* **2008**, *101*, No. 025901.
(34) Reber, D.; Figi, R.; Kühnel, R.-S.; Battaglia, C. Stability of aqueous electrolytes based on LiFSI and NaFSI. *Electrochim. Acta* **2019**, *321*, No. 134644.
(35) Ishai, P. B.; Talary, M. S.; Caduff, A.; Levy, E.; Feldman, Y. Electrode polarization in dielectric measurements: a review. *Meas. Sci. Technol.* **2013**, *24*, No. 102001.
(36) Hess, B.; Kutzner, C.; van der Spoel, D.; Lindahl, E. GROMACS 4: Algorithms for Highly Efficient, Load-Balanced, and Scalable Molecular Simulation. *J. Chem. Theory Comput.* **2008**, *4*, 435−447.
(37) Jorgensen, W. L.; Maxwell, D. S.; Tirado-Rives, J. Development and Testing of the OPLS All-Atom Force Field on Conformational Energetics and Properties of Organic Liquids. *J. Am. Chem. Soc.* **1996**, *118*, 11225−11236.
(38) Canongia Lopes, J. N.; Pádua, A. A. H. Molecular Force Field for Ionic Liquids Composed of Triflate or Bistriflylimide Anions. *J. Phys. Chem. B* **2004**, *108*, 16893−16898.

https://doi.org/10.1021/acs.jpcb.2c02218
J. Phys. Chem. B 2022, 126, 4572−4583

(39) Hess, B.; Bekker, H.; Berendsen, H. J. C.; Fraaije, J. G. E. M. LINCS: A linear constraint solver for molecular simulations. *J. Comput. Chem.* **1997**, *18*, 1463−1472.
(40) Martínez, L.; Andrade, R.; Birgin, E. G.; Martínez, J. M. PACKMOL: A package for building initial configurations for molecular dynamics simulations. *J. Comput. Chem.* **2009**, *30*, 2157−2164.
(41) Hoover, W. G. Canonical dynamics: Equilibrium phase-space distributions. *Phys. Rev. A* **1985**, *31*, 1695−1697.
(42) NOSÉ, S. A molecular dynamics method for simulations in the canonical ensemble. *Mol. Phys.* **2002**, *100*, 191−198.
(43) Berendsen, H. J. C.; Postma, J. P. M.; Gunsteren, W. F.; DiNola, A.; Haak, J. R. Molecular dynamics with coupling to an external bath. *J. Chem. Phys.* **1984**, *81*, 3684−3690.
(44) Raghunathan, A. V.; Aluru, N. R. Self-consistent molecular dynamics formulation for electric-field-mediated electrolyte transport through nanochannels. *Phys. Rev. E* **2007**, *76*, No. 011202.
(45) Nosé, S.; Klein, M. L. Constant pressure molecular dynamics for molecular systems. *Mol. Phys.* **1983**, *50*, 1055−1076.
(46) Parrinello, M.; Rahman, A. Polymorphic transitions in single crystals: A new molecular dynamics method. *J. Appl. Phys.* **1981**, *52*, 7182−7190.
(47) Hansen, J.-P.; McDonald, I. R. *Theory of Simple Liquids*; Hansen, J.-P.; McDonald, I. R., Eds.; Academic Press: Burlington, 2006; p 416.
(48) Kashyap, H. K.; Annapureddy, H. V. R.; Raineri, F. O.; Margulis, C. J. How Is Charge Transport Different in Ionic Liquids and Electrolyte Solutions? *J. Phys. Chem. B* **2011**, *115*, 13212−13221.
(49) Gainaru, C.; Stacy, E. W.; Bocharova, V.; Gobet, M.; Holt, A. P.; Saito, T.; Greenbaum, S.; Sokolov, A. P. Mechanism of Conductivity Relaxation in Liquid and Polymeric Electrolytes: Direct Link between Conductivity and Diffusivity. *J. Phys. Chem. B* **2016**, *120*, 11074−11083.
(50) Stacy, E. W.; Gainaru, C. P.; Gobet, M.; Wojnarowska, Z.; Bocharova, V.; Greenbaum, S. G.; Sokolov, A. P. Fundamental Limitations of Ionic Conductivity in Polymerized Ionic Liquids. *Macromolecules* **2018**, *51*, 8637−8645.
(51) Sangoro, J. R.; Kremer, F. Charge Transport and Glassy Dynamics in Ionic Liquids. *Acc. Chem. Res.* **2012**, *45*, 525−532.
(52) Sangoro, J. R.; Serghei, A.; Naumov, S.; Galvosas, P.; Kärger, J.; Wespe, C.; Bordusa, F.; Kremer, F. Charge transport and mass transport in imidazolium-based ionic liquids. *Phys. Rev. E* **2008**, *77*, No. 051202.
(53) Sangoro, J. R.; Iacob, C.; Naumov, S.; Valiullin, R.; Rexhausen, H.; Hunger, J.; Buchner, R.; Strehmel, V.; Kärger, J.; Kremer, F. Diffusion in ionic liquids: the interplay between molecular structure and dynamics. *Soft Matter* **2011**, *7*, 1678−1681.
(54) Dyre, J. C.; Maass, P.; Roling, B.; Sidebottom, D. L. Fundamental questions relating to ion conduction in disordered solids. *Rep. Prog. Phys.* **2009**, *72*, No. 046501.
(55) Maass, P.; Meyer, M.; Bunde, A. Nonstandard relaxation behavior in ionically conducting materials. *Phys. Rev. B* **1995**, *51*, 8164−8177.
(56) Roling, B.; Martiny, C.; Brückner, S. Ion transport in glass: Influence of glassy structure on spatial extent of nonrandom ion hopping. *Phys. Rev. B* **2001**, *63*, No. 214203.
(57) Popov, I.; Biernacka, K.; Zhu, H.; Nti, F.; Porcarelli, L.; Wang, X.; Khamzin, A.; Gainaru, C.; Forsyth, M.; Sokolov, A. P. Strongly Correlated Ion Dynamics in Plastic Ionic Crystals and Polymerized Ionic Liquids. *J. Phys. Chem. C* **2020**, *124*, 17889−17896.
(58) Angell, C. A. Diffusion—Conductance Relations and Free Volume in Molten Salts. *J. Phys. Chem. A* **1965**, *69*, 399−403.
(59) Bockris, J. O. M.; Hooper, G. W. Self-diffusion in molten alkali halides. *Discuss. Faraday Soc.* **1961**, *32*, 218−236.
(60) Harris, K. R. Relations between the Fractional Stokes−Einstein and Nernst−Einstein Equations and Velocity Correlation Coefficients in Ionic Liquids and Molten Salts. *J. Phys. Chem. B* **2010**, *114*, 9572−9577.
(61) Marcolongo, A.; Marzari, N. Ionic correlations and failure of Nernst-Einstein relation in solid-state electrolytes. *Phys. Rev. Mater.* **2017**, *1*, No. 025402.
(62) Murch, G. E. The haven ratio in fast ionic conductors. *Solid State Ionics* **1982**, *7*, 177−198.
(63) Murch, G. E. The Nernst-Einstein equation in high-defect-content solids. *Philos. Mag. A* **1982**, *45*, 685−692.
(64) Spedding, P. L.; Mills, R. Trace-Ion Diffusion in Molten Alkali Carbonates. *J. Electrochem. Soc.* **1965**, *112*, No. 594.
(65) Vargas-Barbosa, N. M.; Roling, B. Cover Feature: Dynamic Ion Correlations in Solid and Liquid Electrolytes: How Do They Affect Charge and Mass Transport? (ChemElectroChem 2/2020). *ChemElectroChem* **2020**, *7*, 363.
(66) Yokota, I. On the Deviation from the Einstein Relation Observed for Diffusion of Ag+ Ions in α-Ag2S and Others. *J. Phys. Soc. Jpn.* **1966**, *21*, 420−423.
(67) MacFarlane, D. R.; Forsyth, M.; Izgorodina, E. I.; Abbott, A. P.; Annat, G.; Fraser, K. On the concept of ionicity in ionic liquids. *Phys. Chem. Chem. Phys.* **2009**, *11*, 4962−4967.
(68) Noda, A.; Hayamizu, K.; Watanabe, M. Pulsed-Gradient Spin−Echo 1H and 19F NMR Ionic Diffusion Coefficient, Viscosity, and Ionic Conductivity of Non-Chloroaluminate Room-Temperature Ionic Liquids. *J. Phys. Chem. B* **2001**, *105*, 4603−4610.
(69) Braun, M.; Kehr, K. W. Diffusivity and mobility of lattice gases in lattices with randomly blocked sites. *Philos. Mag. A* **1990**, *61*, 855−871.
(70) Isard, J. O. The Haven ratio in glasses. *J. Non-Cryst. Solids* **1999**, *246*, 16−26.
(71) Murch, G. E.; Dyre, J. C. Correlation effects in tracer diffusion and ionic conductivity. *Solid State Ionics* **1986**, *20*, 203−207.
(72) Zhang, Z.; Wheatle, B. K.; Krajniak, J.; Keith, J. R.; Ganesan, V. Ion Mobilities, Transference Numbers, and Inverse Haven Ratios of Polymeric Ionic Liquids. *ACS Macro Lett.* **2020**, *9*, 84−89.
(73) Terai, R.; Hayami, R. Ionic diffusion in glasses. *J. Non-Cryst. Solids* **1975**, *18*, 217−264.
(74) Every, H. A.; Bishop, A. G.; MacFarlane, D. R.; Orädd, G.; Forsyth, M. Transport properties in a family of dialkylimidazolium ionic liquids. *Phys. Chem. Chem. Phys.* **2004**, *6*, 1758−1765.
(75) Harris, K. R.; Kanakubo, M. Self-Diffusion Coefficients and Related Transport Properties for a Number of Fragile Ionic Liquids. *J. Chem. Eng. Data* **2016**, *61*, 2399−2411.
(76) Seki, S.; Hayamizu, K.; Tsuzuki, S.; Fujii, K.; Umebayashi, Y.; Mitsugi, T.; Kobayashi, T.; Ohno, Y.; Kobayashi, Y.; Mita, Y.; et al. Relationships between center atom species (N, P) and ionic conductivity, viscosity, density, self-diffusion coefficient of quaternary cation room-temperature ionic liquids. *Phys. Chem. Chem. Phys.* **2009**, *11*, 3509−3514.
(77) Stolwijk, N. A.; Obeidi, S. Combined analysis of self-diffusion, conductivity, and viscosity data on room temperature ionic liquids. *Electrochim. Acta* **2009**, *54*, 1645−1653.
(78) Tokuda, H.; Hayamizu, K.; Ishii, K.; Susan, M. A. B. H.; Watanabe, M. Physicochemical Properties and Structures of Room Temperature Ionic Liquids. 2. Variation of Alkyl Chain Length in Imidazolium Cation. *J. Phys. Chem. B* **2005**, *109*, 6103−6110.
(79) Choi, U. H.; Lee, M.; Wang, S.; Liu, W.; Winey, K. I.; Gibson, H. W.; Colby, R. H. Ionic Conduction and Dielectric Response of Poly(imidazolium acrylate) Ionomers. *Macromolecules* **2012**, *45*, 3974−3985.
(80) Turton, D. A.; Hunger, J.; Stoppa, A.; Hefter, G.; Thoman, A.; Walther, M.; Buchner, R.; Wynne, K. Dynamics of Imidazolium Ionic Liquids from a Combined Dielectric Relaxation and Optical Kerr Effect Study: Evidence for Mesoscopic Aggregation. *J. Am. Chem. Soc.* **2009**, *131*, 11140−11146.
(81) Schoenert, H. J. Evaluation of velocity correlation coefficients from experimental transport data in electrolytic systems. *J. Phys. Chem. B* **1984**, *88*, 3359−3363.
(82) Dong, D.; Sälzer, F.; Roling, B.; Bedrov, D. How efficient is Li+ ion transport in solvate ionic liquids under anion-blocking conditions in a battery? *Phys. Chem. Chem. Phys.* **2018**, *20*, 29174−29183.
(83) Harris, K. R. Can the Transport Properties of Molten Salts and Ionic Liquids Be Used To Determine Ion Association? *J. Phys. Chem. B* **2016**, *120*, 12135−12147.

https://doi.org/10.1021/acs.jpcb.2c02218
J. Phys. Chem. B 2022, 126, 4572−4583

(84) McDaniel, J. G.; Son, C. Y. Ion Correlation and Collective Dynamics in BMIM/BF4-Based Organic Electrolytes: From Dilute Solutions to the Ionic Liquid Limit. *J. Phys. Chem. B* **2018**, *122*, 7154−7169.

https://doi.org/10.1021/acs.jpcb.2c02218
J. Phys. Chem. B 2022, 126, 4572−4583